Electronic Supplementary Material (ESI) for Journal of Materials Chemistry A.

Great Improvement in the Performance and Lifetime of a Fuel Cell Using a Highly Dense, Well-Ordered, and Cone-Shaped Nafion Array

Fandi Ning,[1,2,3] Chuang Bai,[1,2] Jiaqi Qin,[4] Yujiang Song,[4] Ting Zhang,[2] Jiafan Chen,[5] Jun Wei,[2] Guanbin Lu,[2] Huihui Wang,[1,2] Yali Li,[2] Junnan Gu,[2] Yangbin Shen,[6] Yi Cui,[1,3] Yunjie Huang,[7] and Xiaochun Zhou[1,2,8]*

1. School of Nano Technology and Nano Bionics, University of Science and Technology of China, Hefei 230026, China.
2. Division of Advanced Nanomaterials, Suzhou Institute of Nano-tech and Nano-bionics, Chinese Academy of Sciences (CAS), Suzhou 215123, China
3. Vacuum Interconnected Workstation, Suzhou Institute of Nano-tech and Nano-bionics, Chinese Academy of Sciences (CAS), Suzhou 215123, China
4. State Key Laboratory of Fine Chemicals, School of Chemical Engineering, Dalian University of Technology, Dalian, Liaoning 116024, China
5. Platform of Characterization & Analysis, Suzhou Institute of Nano-tech and Nano-bionics, Chinese Academy of Sciences (CAS), Suzhou 215123, China
6. Institute of Materials Science and Devices, Suzhou University of Science and Technology, Suzhou 215009, China
7. Faculty of Materials Science and Chemistry, China University of Geosciences, Wuhan 430074, C hina
8. Key Lab of Nanodevices and Applications, Suzhou Institute of Nano-Tech and Nano-Bionics, Chinese Academy of Sciences (CAS), Suzhou 215123, China.

Correspondence and requests for materials should be addressed to X. Z. (email: xczhou2013@sinano.ac.cn).

Content

SI-1. Schematic of three generations of MEA.

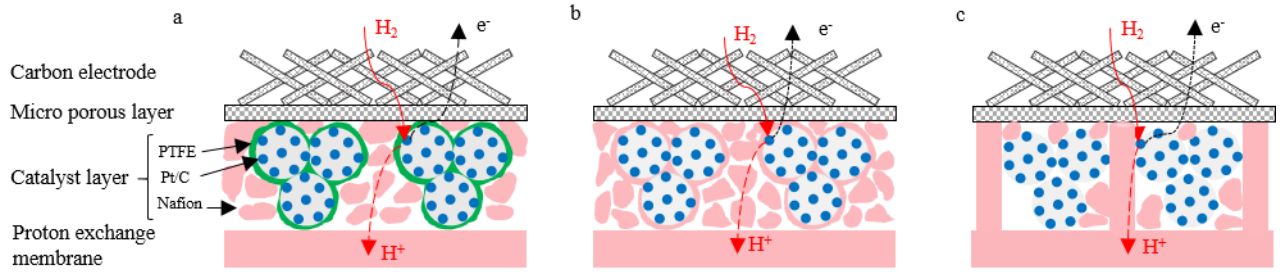

Figure S1. Schematic of three generations of MEA. (a) The first generation GDE MEA. (b) The second generation CCM MEA. (c) The third generation ordered catalyst layer MEA.

For the first generation of MEA, as shown in **Figure S1**a, the catalyst ink composed with catalyst and polytetrafluoroethylene (PTFE) was coated on carbon paper electrode to prepare catalyst layer. Then the catalyst layer was immersed with proton conductor (such as Nafion) to produce proton conduct pathways. However, there are two problems at this stage: PTFE occupies a part of active site of catalyst; Nafion cannot penetrate into the inner part of the catalyst layer.

For the second generation of MEA, as shown in **Figure S1**b, PTFE is total replaced by Nafion in the catalyst ink. However, the content of proton conductor in the catalyst layer cannot increase indefinitely, because excessive Nafion will occupies the volume of the catalyst. Excess Nafion will lower down the performance of PEMFC.

The third generation ordered catalyst layer MEA. In order to further increase the Nafion content and proton conductivity in the catalyst layer. Y. Zhang et al.[1] etched the surface of Nafion 117 membrane with nano-lithography technology, and obtained a large three-phase interface, which improved the utilization rate of the catalyst. M. Aizawa et al.[2] prepared many regular bulges on the surface of Nafion membrane by transfer printing or microinjection. However, in these methods, the Nafion phase has a huge volume (from several microns to tens of microns), which plays a more similar role in increasing the contact area between the catalyst layer and the membrane. More importantly, it is difficult for the Nafion phase to penetrate into the inner of catalyst layer uniformly, and the structure of the membrane is destroyed to varying degrees.

SI-2. SEM of AAO with different length.

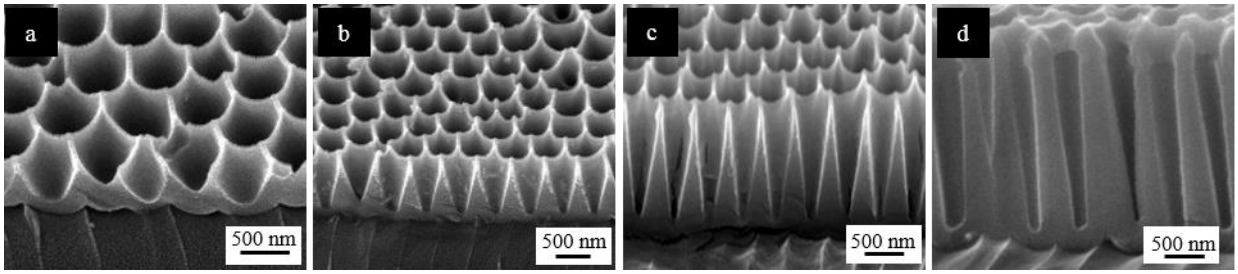

Figure S2. SEM of AAO with different length. (a) The channel depth of AAO is 0.5 μm. (b) The channel depth of AAO is 0.9 μm. (c) The channel depth of AAO is 1.3 μm. (d) The channel depth of AAO is 2.5 μm.

SI-3. Calculation of cone and rod-shaped Nafion array density.

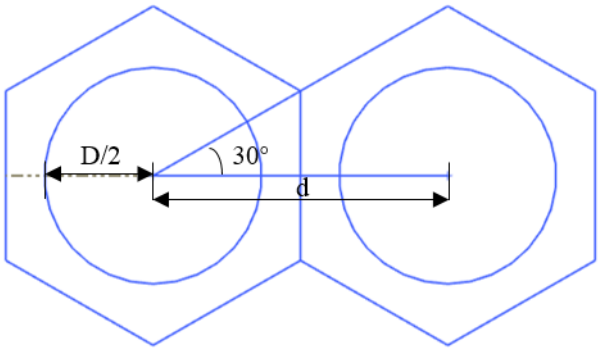

Figure S3. Arrangement hole model of AAO template.

The holes of AAO are arranged in density according to regular hexagon.[3]

For the area of a regular hexagon is: $S = \frac{3}{2}\sqrt{3}a^2$

Where a is the edge length of a regular hexagon.

For $a = d \times \tan 30^{\circ}$

Submit to form equation: $S = \frac{\sqrt{3}}{2}d^2$

So, the hole density is: $\frac{2}{\sqrt{3}} \times \frac{1}{d^2}$

For cone-shaped AAO，d is 4.5×10^{-5} cm, so the density is 5.7×10^{8} cones/cm^2.

For rod-shaped AAO，d is 3.0×10^{-5} cm, so the density is 1.3×10^{9} rods/cm^2.

SI-4. Contact angle of Nafion emulsion (DMSO as solvent) with AAO.

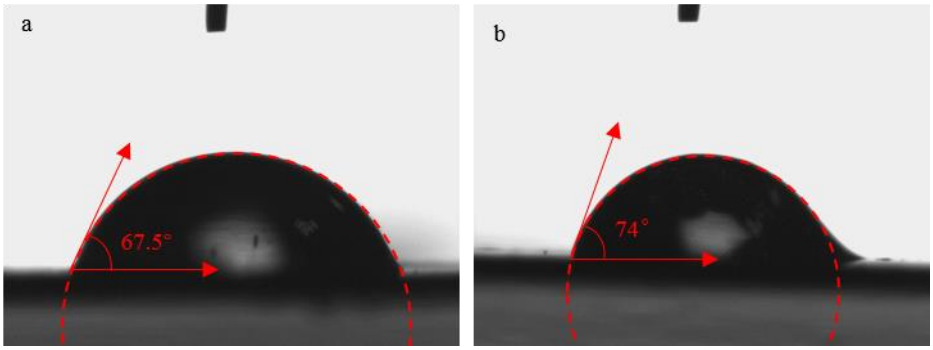

Figure S4. Contact angle of Nafion emulsion (DMSO as solvent) with AAO. (a) Nafion emulsion has a mass fraction of 2.5%. (b) Nafion emulsion has a mass fraction of 20%.

The contact angles of Nafion emulsion (mass fraction of 2.5% and 20%) with AAO are 67.5°, 74°, respectively. The contact angle indicates that under normal pressure and no surfactant, Nafion emulsion cannot be completely spread on the surface of AAO. Filling rate of Nafion emulsion cannot be guaranteed.

SI-5. Formation of Nafion membrane during dropping of Nafion emulsion.

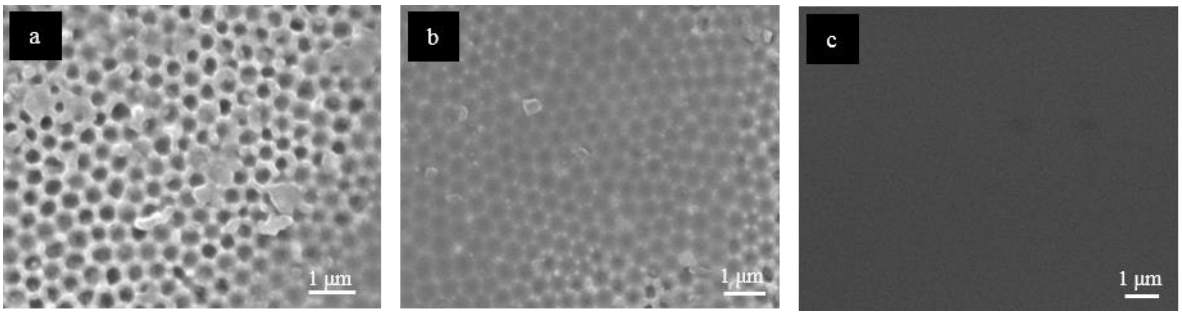

Figure S5. Front SEM of proton conductor array of Nafion membrane along with the dropping of Nafion emulsion. (a) The volume of Nafion emulsion drops is 20 μL. (b) The volume of Nafion emulsion drops is 50 μL. (c) The volume of Nafion emulsion drops is 100 μL.

As the Nafion emulsion is further added during the curing process, a uniform Nafion membrane is formed on the surface of the AAO slowly as shown in **Figure S5** a, b, c, and the front surface of the Nafion membrane has no obvious protrusions and depressions.

SI-6. High aspect ratio Nafion array.

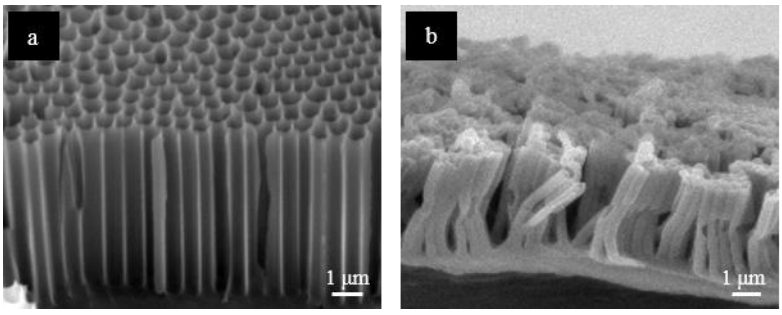

Figure S6. High aspect ratio Nafion array. (a) The cross section SEM of AAO, (b) The cross section SEM of corresponding Nafion array.

By changing the channel morphology of AAO, the corresponding morphology of the Nafion array can be obtained. From **Figure S6**a, it can be seen that the channel morphology of AAO is cylindrical, and the corresponding Nafion array in **Figure S6**b is cylindrical. From **Figure S6**a, AAO has a channel depth of 5 μm, a pore diameter of 300 nm, a pore spacing of 450 nm and a length diameter aspect ratio (H/D) of 16.7. From **Figure S6**b, Nafion array size matches AAO size, Nafion array has a high aspect ratio of 16.7.

SI-7. Unique properties of Nafion array on the Nafion membrane

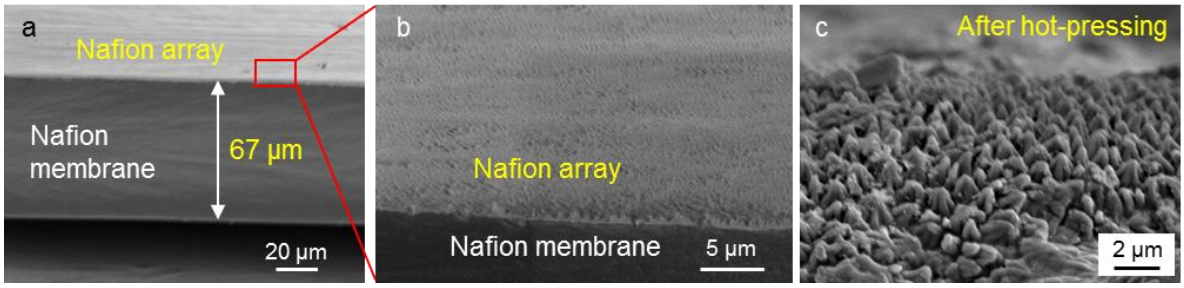

Figure S7. Unique properties of Nafion array on the Nafion membrane. (a) The cross section of Nafion membrane with Nafion array. (b) Zoom in one part of a. (c) SEM image of Nafion array after hot-pressing and water immersing.

The above excellent performance of PEMFCs made by Nafion array is based on the unique properties of the array and our robust optimizations, which will be introduced in detail below. In order to understand the relative size of the Nafion array to the membrane, and the uniformity of the Nafion array, we further characterize the Nafion array on Nafion membrane by SEM at different scales. **Figure S7**a shows that the thickness of membrane is 67 μm, while the height of the Nafion array is only 1.3 μm, indicating a 52 times difference between them. The Nafion array exhibits like a very thin and dense brush on the membrane. **Figure S7**a also shows that the top of Nafion membrane is fully covered by the Nafion array, whose color is white. The distribution of the Nafion array on the Nafion membrane is pretty homogeneous in large scale in **Figure S7**a. When we zoom in the top of the cross-section in **Figure S7**b, we can see that the distribution of the Nafion array on the Nafion membrane is also pretty homogeneous in smaller scale.

In order to discover the tolerance of Nafion arrays to hot-pressing operation, we first hot press the arrays, and then deep them into water. **Figure S7**c shows that the shape and density of the array can be well maintained even after hot pressing. This unique property indicates that the Nafion array will not be destroyed during normal hot-pressing operation, which provides an outstanding condition for the preparation of MEA. The unique advantages of the Nafion array mentioned above provide an ability to make high performance PEMFC.

SI-8. TEM of Pt prepared by sputtering.

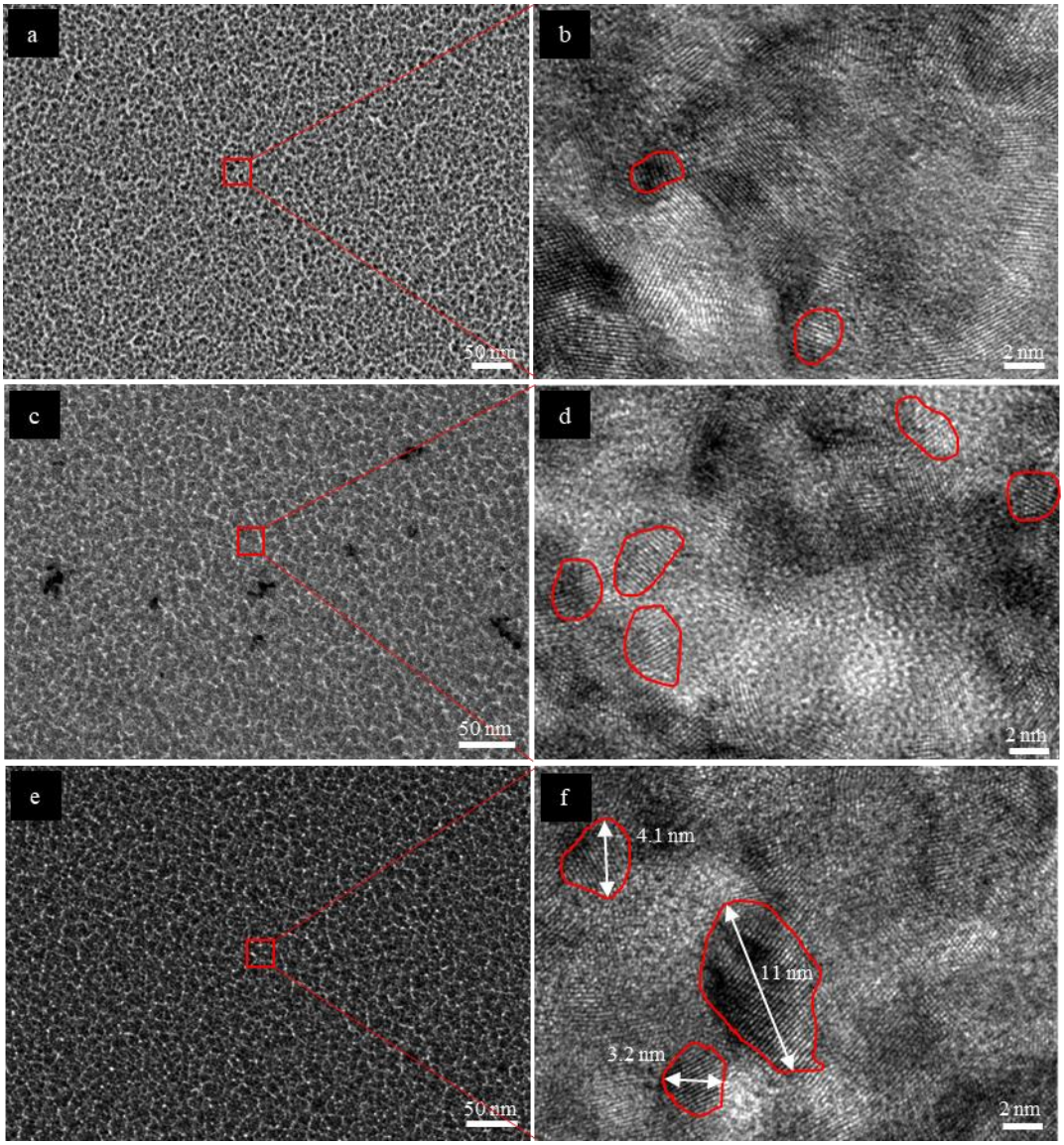

Figure S8. TEM of Pt prepared by sputtering. (a) TEM of Pt prepared by sputtering. The loading of Pt is 8.1 μg cm^{-2}. (b) High-resolution TEM of (a). (c) TEM of Pt prepared by sputtering. The loading of Pt is 17.6 μg cm^{-2}. (d) High-resolution TEM of (c). (e) TEM of Pt prepared by sputtering. The loading of Pt is 49.6 μg cm^{-2}. (f) High-resolution TEM of (e).

It can be seen from TEM that Pt particles prepared by magnetron sputtering actually form Pt thin film, and there are many amorphous Pt zones. Therefore, the size of Pt particles can only be considered along the crystal plane about 3-5 nm.

SI-9. Element mapping of Nafion membrane with Nafion array after loading Pt.

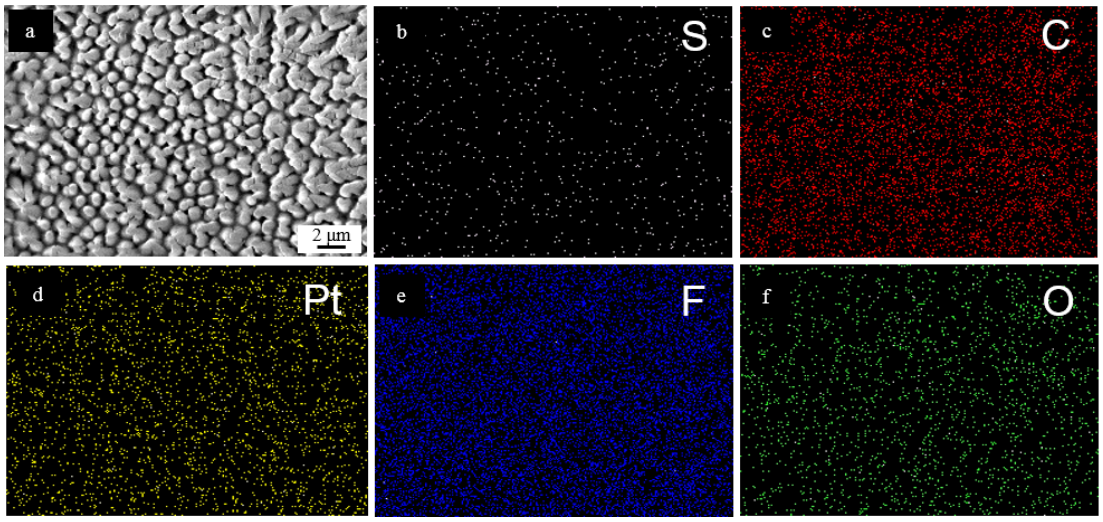

Figure S9. Element mapping of Nafion membrane with Nafion array after loading Pt. (a) Element mapping selected area. (b) Mapping of element S, the color is white. (c) Mapping of element C, the color is red. (d) Mapping of element Pt, the color is yellow. (e) Mapping of element F, the color is bule. (f) Mapping of element O, the color is green. The element mapping of the proton conductor array after loading Pt shows that Pt has a relatively uniform load, and C, S, F, and O correspond to Nafion.

SI-10. Optimizing the Pt loading on Nafion array

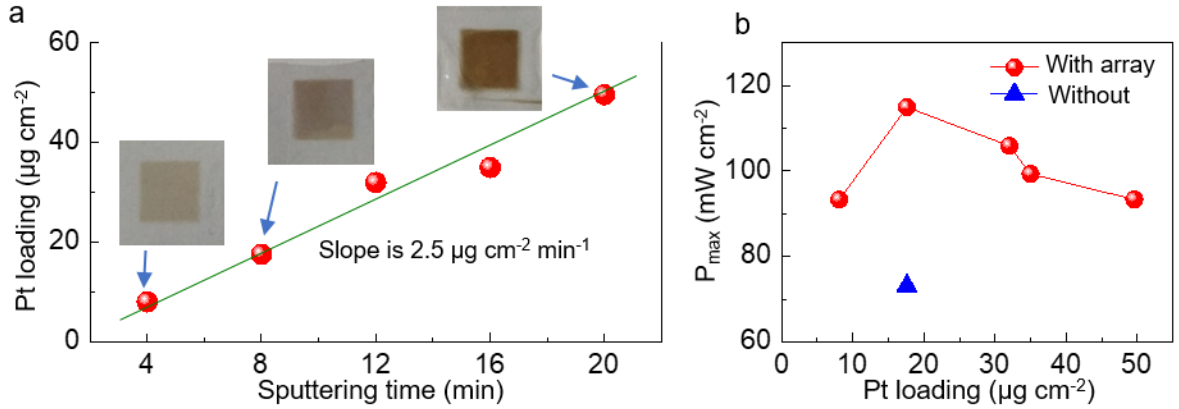

Figure S10. Optimizing the Pt loading on cone Nafion array. (a) Relationship between sputtering time and Pt loading. The inserts are the photo picture of Nafion membrane with Nafion array after sputtering Pt. (b) Peak power density (P_{max}) of fuel cells under different Pt loading.

Pt loading is the key parameter to affect the performance of PEMFC. Here, we adjust Pt loading by varying the sputtering time at a constant sputtering current of 20 mA. The relationship between the sputtering time and the load of Pt can be seen in **Figure S10**a, which shows that the corresponding Pt load increased from 8.1 to 49.6 μg cm^{-2} by changing the sputtering time for 4-20 min. By fitting the points with a linear function, the slope can be obtained as 2.5 μg cm^{-2} min^{-1}. With the increase of Pt loading, the color of Pt loading area on Nafion changed from light yellow to deep brown (inserts in **Figure S10**a). Pt nanoparticles obtained by magnetron sputtering are small 3-11 nm (SI-9 and SI-18). Due to the small size and low loading of Pt nanocatalyst on the Nafion array, we did not find the characteristic peaks of Pt by XRD (Figure S18).

The relationship between P_{max} and the Pt loading is shown in **Figure S10b**. The polarization curves of the fuel cells are shown in Figure S19. Generally, there is an optimal Pt loading. When the load of Pt increases from 8.1 to 17.6 μg cm^{-2}, the peak power density increases from 93 to 115 mW cm^{-2}. The improvement of fuel cells performances is attributed to the increase of Pt loading and catalytic active sites. However, when the Pt loading increase from 17.6 to 49.6 μg cm^{-2}, the peak power density decreases from 115 to 93 mW cm^{-2}. The main reason for the decrease of fuel cell performance may be due to the decrease of specific surface area of Pt with the increase of Pt loading. Since the specific surface area of Pt is strongly proportional to its catalytic activity, the fuel cells performance degrades at high Pt loading.

SI-11. Optical photo of graphene nanosheet dispersion.

Figure S11. Optical photo of graphene nanosheet dispersion. The concentration of the graphene nanosheet dispersion is 0.529 mg/mL. Graphene nanosheet dispersion is a black homogeneous dispersion solution with no obvious precipitation.

SI-12. Preparation procedure of rod-shaped array and the corresponding MEA.

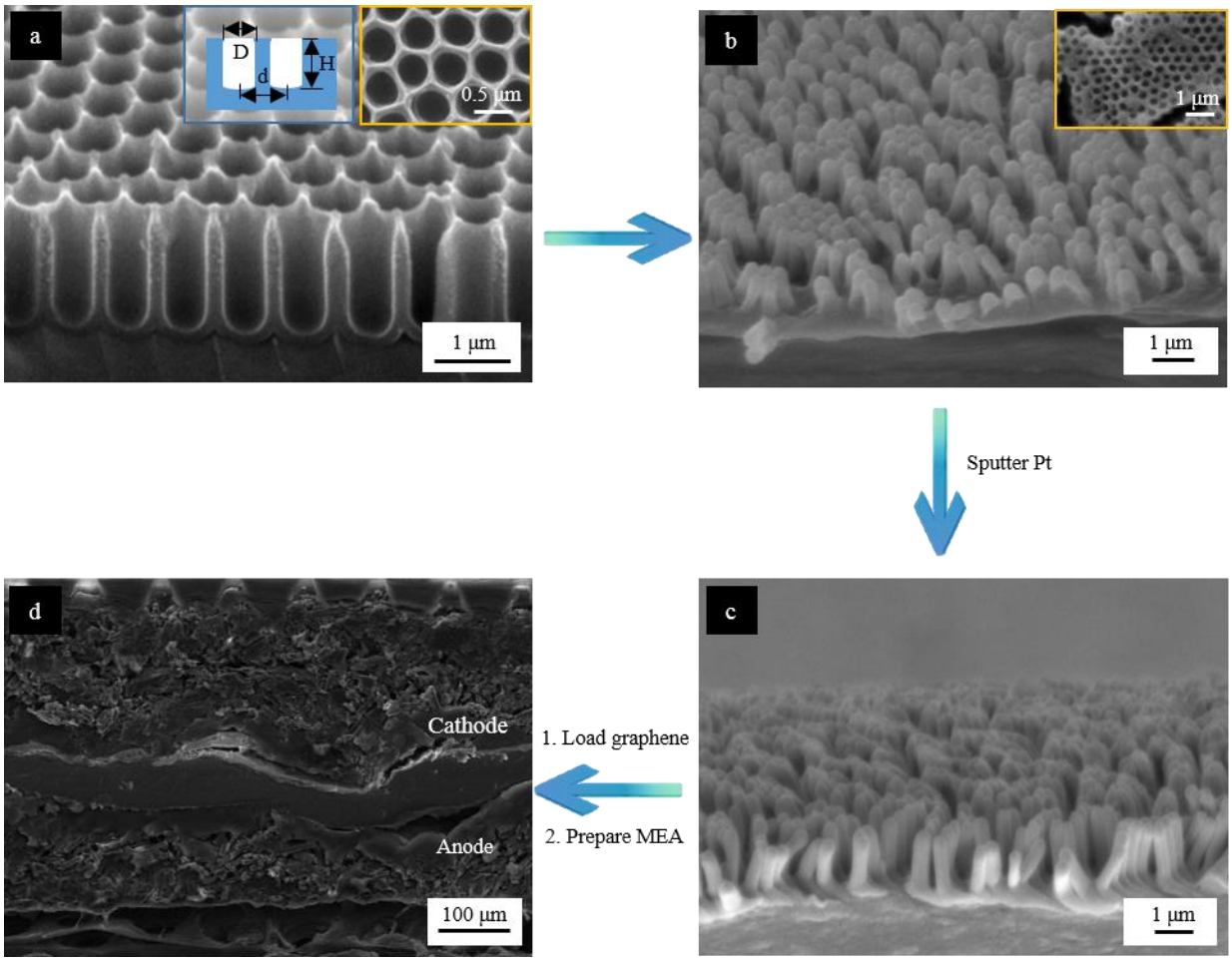

Figure S12. Preparation procedure of rod-shaped array and the corresponding MEA. (a) SEM image of cross-section of AAO template. The insert is the top view of AAO and schematic of AAO. (b) SEM image of Nafion array after removing AAO template. The insert is the top view of the array. (c) SEM image of Nafion array loaded with Pt nanocatalyst. (d) SEM image of the cross-section of the MEA made by the Nafion array with graphene and Pt catalyst.

SI-13. SEM of Nafion array of 0.9 um in length.

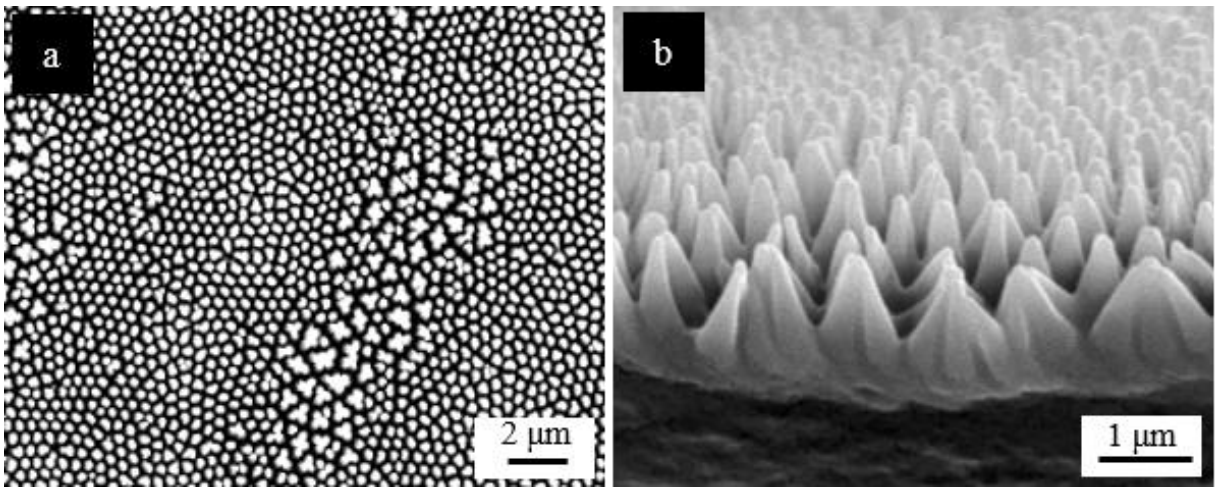

Figure S13. SEM of Nafion array of 0.9 um in length. (a) Frontal SEM of the Nafion array with length of 0.9 um. (b) Cross-section SEM of the Nafion array with length of 0.9 um.

It can be seen from **Figure S13** a and b, some of the Nafion arrays are clustered in bundles, others are not clustered, but exist alone. Besides, the bundles are not large, and there are not many bundles of regions.

SI-14. The polarization curves of fuel cell with different length of cone-shaped Nafion array.

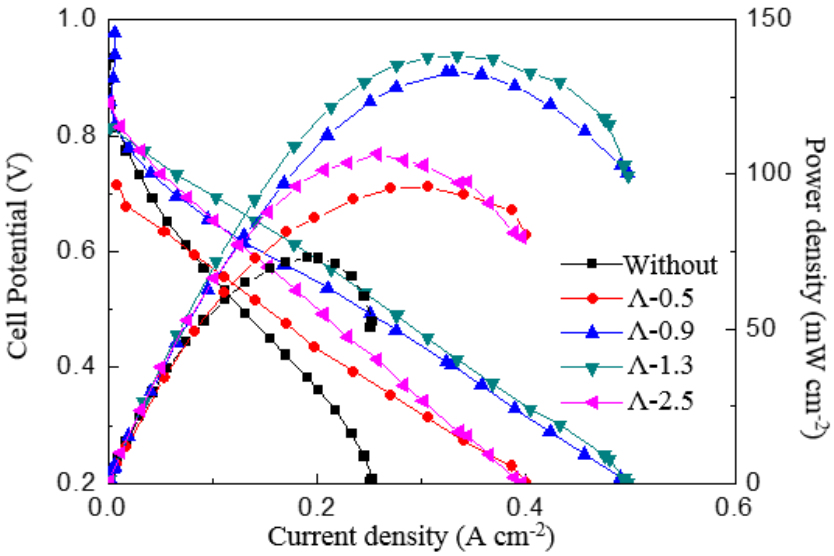

Figure S14. The polarization curves of fuel cell with different length of cone-shaped Nafion array.

SI-15. Calculation of Pt size at 16.7 μg cm^{-2} Pt loading.

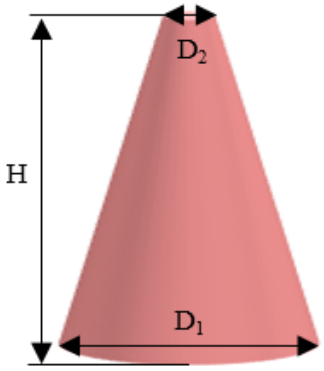

Figure S15. Schematic diagram of cone-shaped array.

The load area of Pt particles is divided into two parts, one part is loaded in the Nafion array part and the other is loaded in the non-array part.

For the Nafion array zone, the area of Pt loaded on a single Nafion cone is:

$$S_1 = \pi \times \frac{{D_2}^2}{4} + \pi \times \frac{D_1}{2} \times l + \pi \times \frac{D_2}{2} \times l$$

Where, $l = \sqrt{\left(\frac{D_1}{2} - \frac{D_2}{2}\right)^2 + H^2}$

For, D_1 is 0.4 μm, D_2 is 0.1 μm, H is 0.5 μm,

So, $l = 0.522\mu m^2$,

So, $S_1 = 0.418\mu m^2$,

For the density of cone-shaped Nafion array is $5.7\times10^8/cm^2$,

Thus, the load area of Pt on the Nafion array is 2.38×10^8 μm^2 $/cm^2$,

For the non-Nafion array zone, the area of Pt loaded is total area minus the area at the bottom of the array.

The bottom area of a single Nafion cone is: $S_{bottom} = \pi \times \frac{{D_1}^2}{4}$,

So, $S_{bottom} = 0.1256\mu m^2$,

Therefore, the bottom area of all Nafion arrays is: 0.716×10^8 μm^2,

Thus, non-Nafion array zone, the area of Pt loaded is 0.284 cm^2,

Thus, the total load area of the Nafion array Pt is 2.66 cm^2,

For the density of Pt is 21.5 g/cm^3,

Thus, the size of Pt is 3.1 nm

SI-16. Calibration of graphene nanosheet dispersion concentration.

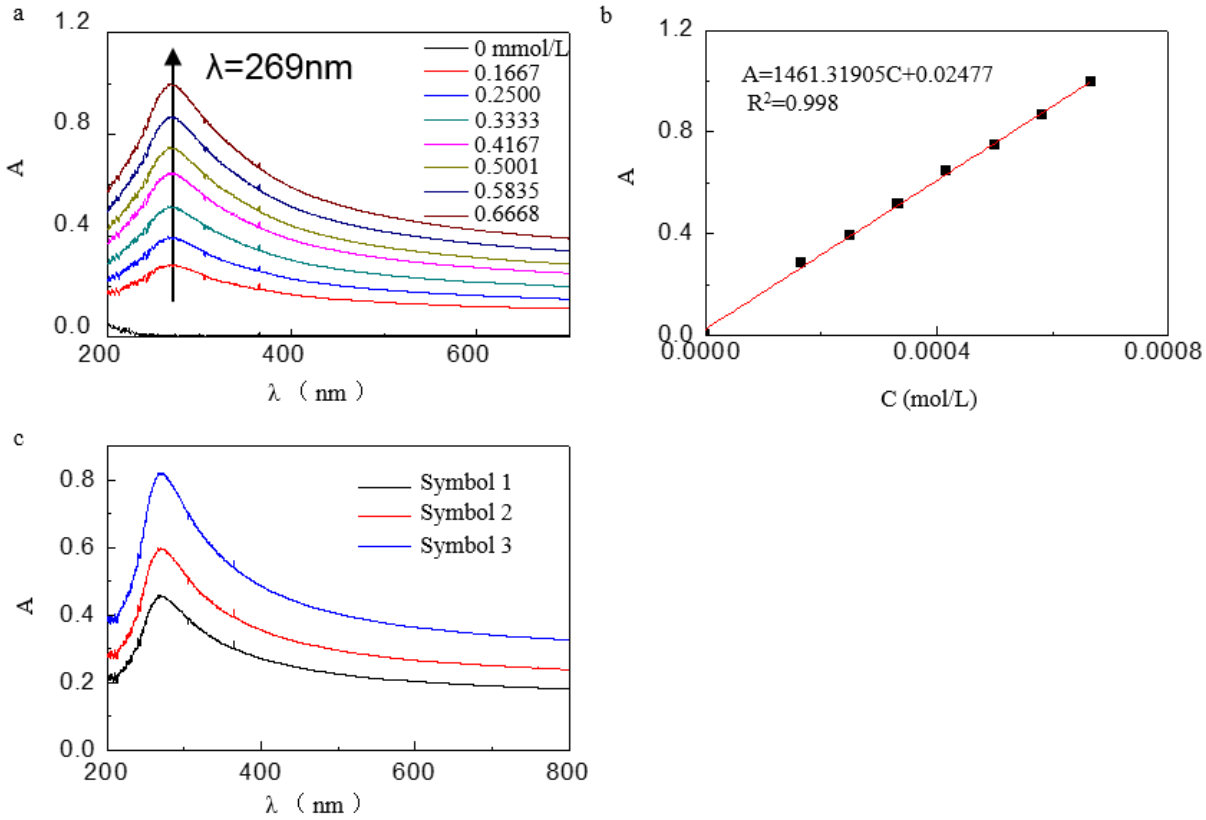

Figure S16. Calibration of graphene dispersion concentration. (a) UV–Vis of different concentrations of graphene nanosheet dispersion. (b) Linear fit of absorbance at 269 nm. (c) UV–Vis of sprayed graphene dispersion.

The concentration of the sprayed graphene nanosheet is 0.529 mg/mL. The concentration of the sprayed graphene nanosheet is the average of the three samples.[4]

SI-17. Raman spectroscopy of graphene nanosheet.

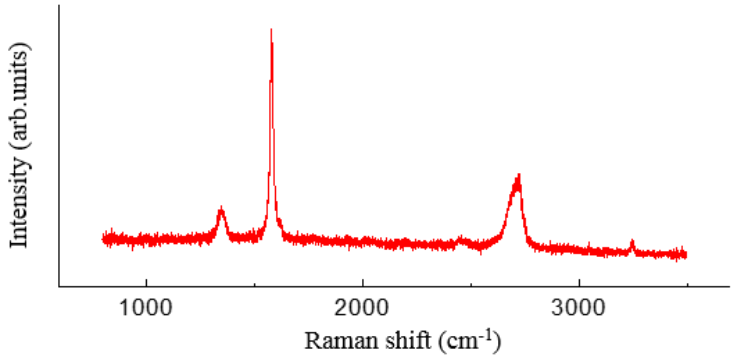

Figure S17. Raman spectroscopy of graphene nanosheet.

D peak: the peak area near 1350 cm^{-1} is 3193.46. This peak is the disordered vibration peak of graphene. It is caused by the lattice vibration leaving the center of Brillouin zone. It is used to characterize the structural defects of graphene samples.

G peak: the peak area near 1580 cm^{-1} is 6441.75, which is caused by in-plane vibration of SP^2 carbon atoms.

Generally, the strength ratio of D peak to G peak (I_D/I_G) is used to characterize the defect density of graphene. The smaller the strength, the less the defect.[5]

Thus, I_D/I_G is 0.5, the smaller I_D/I_G value means that graphene has smaller defects.

SI-18. Optical photo of Nafion membrane after loading graphene.

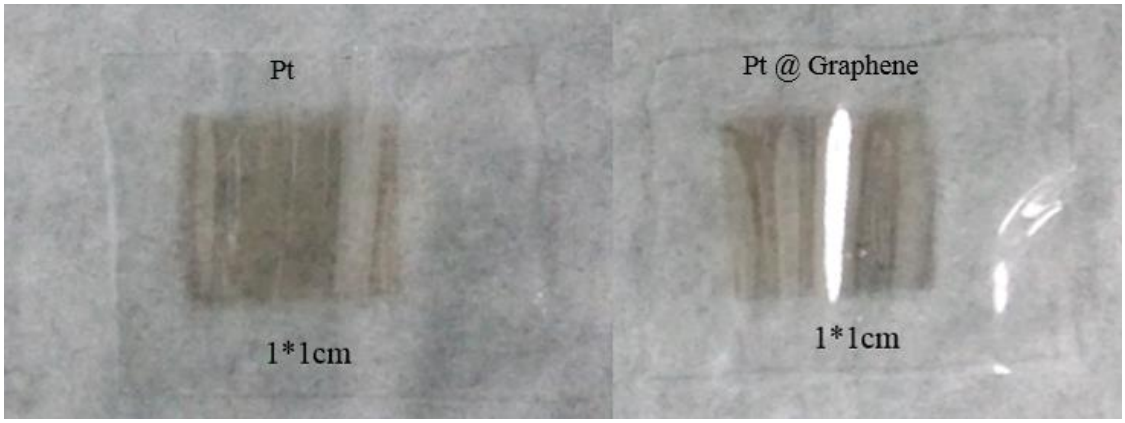

Figure S18. Optical photograph of Nafion membrane after loading graphene. The loadings of Pt and graphene are 8.1 and 7.92 μg cm^{-2}, respectively.

From the optical photo, the graphene loading did not bring about significant changes in Nafion membrane, which means that the graphene loading did not damage Nafion membrane.

SI-19. The polarization curves of PEMFCs with different graphene nanosheet loading

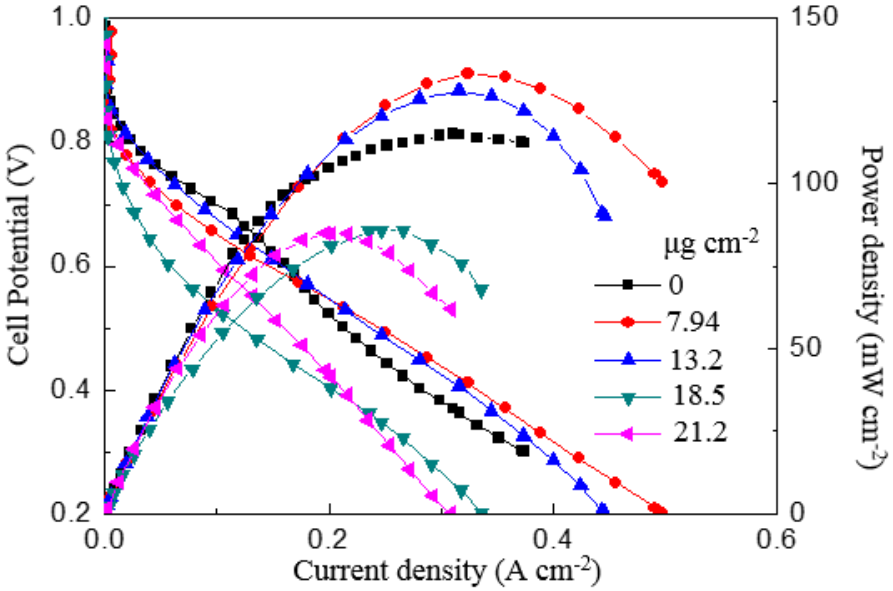

Figure S19. The polarization curves of PEMFCs with different graphene nanosheet loding.

SI-20. EDX of fuel cell cross section before and after constant current discharge.

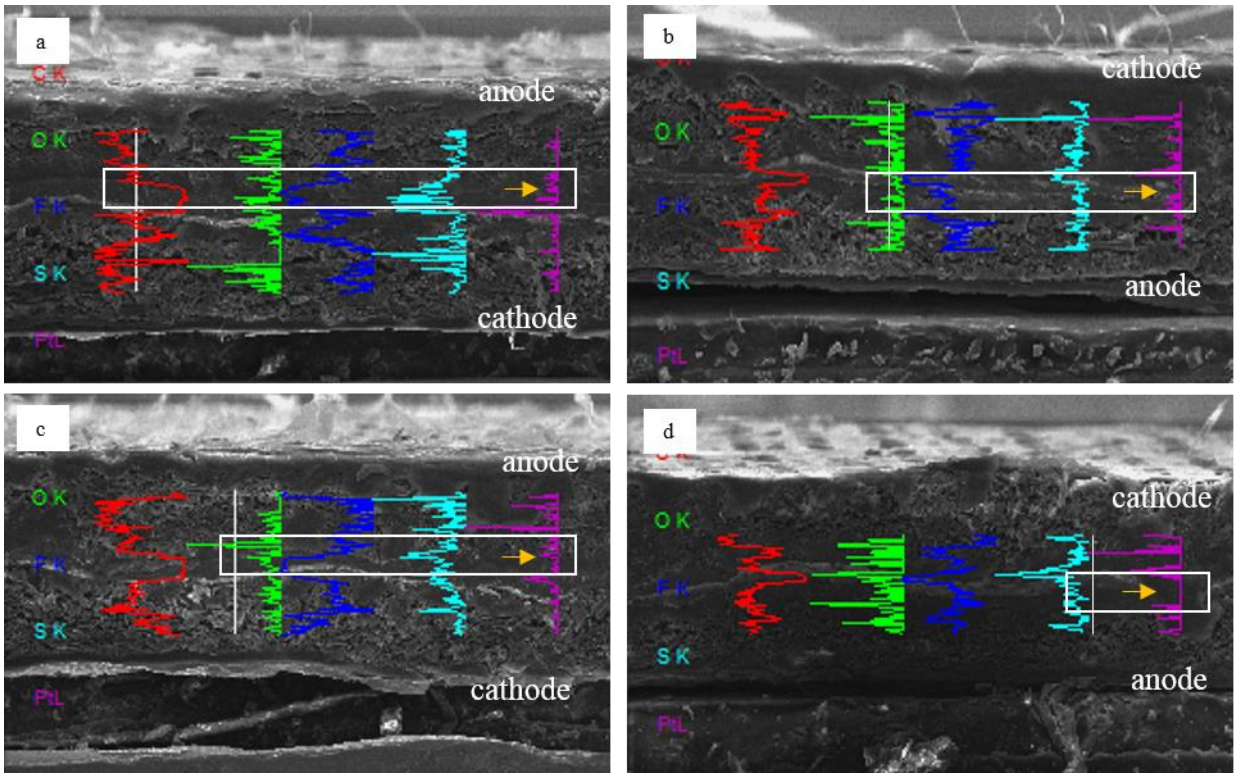

Figure S20. EDX of fuel cell cross section before and after constant current discharge. (a), (b) The cross section of fuel cell with rod shaped proton conductor array before (a) and after (b) constant current discharge. (c), (d) The cross section of fuel cell with cone shaped proton conductor array before (c) and after (d) constant current discharge.

SI-21. Summarized the literatures to compare the characteristic parameters

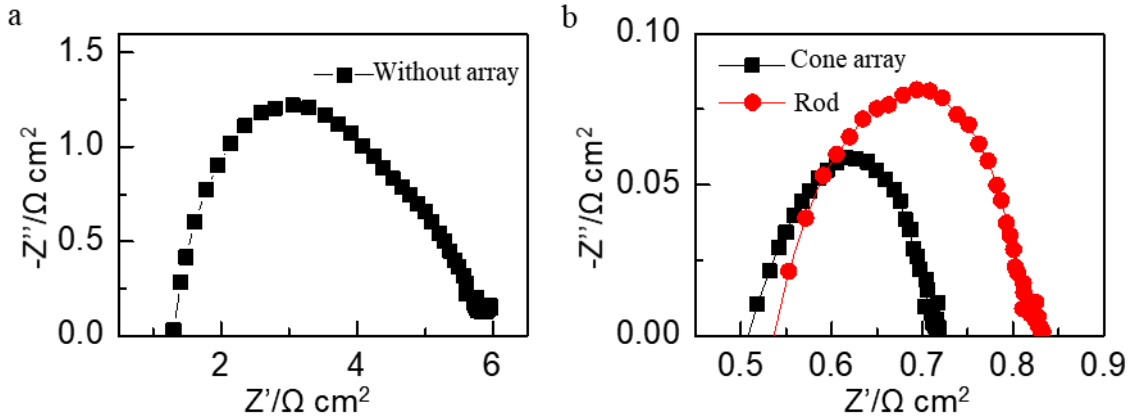

Figure S21. Impedance Spectroscopy (EIS) of fuel cell without Nafion array, with cone-shaped and rod-shaped Nafion array. (a) EIS of fuel cell without Nafion array. (b) EIS of fuel cell without Nafion array, with cone-shaped and rod-shaped Nafion array.

The EIS measurements were performed at open-circuit voltage (OCV) in the frequency range of 100 kHz to 0.01 Hz, and at an amplitude of the sinusoidal voltage signal of 5 mV. The gas on both sides of the anode and cathode is hydrogen, and the flow rate of hydrogen was 15 mL/min. The cathode served as the working electrode whereas the anode served as the counter electrode and reference electrode.

From **Figure S21**a and b, the fuel cell with Nafion array had a smaller semicircular loop than that without Nafion array which revealing that the fuel cell with Nafion array had the lower charge transfer resistance. Meanwhile, form **Figure S21**b, the fuel cell with cone-shaped array had a smaller semicircular loop than rod-shaped array, which also means cone-shaped Nafion array had the lowest charge transfer resistance.

SI-22. Summarized the literatures to compare the characteristic parameters

Table S1. PEMFCs based on Nafion array

Template or array type	Maximum power density		Pt loading (mg cm^{-2})	Operating temperature (°C)	Gas feed	Ref.
	(mW cm^{-2})	(kW $g_{Pt,array}^{-1}$)				
Polycarbonate membrane (diameter and length:200 nm and 10 μm)	106	0.24	0.439 at cathode	80	H_2/air	6
Hybrid polymer with Nafion and PPy	800	11.97	0.065 at cathode	70	H_2/O_2	7
Patterned poly(cyanomethyl acrylate) template	240	1.2	0.2 at cathode	50	H_2/O_2	8
Electron beam lithography and dry etching strategies, Nafion pattern	22.1	-	-	room temperature	H_2/O_2	9
Imprint/micro mold lithography, Nafion array	320	1.1	0.3 at cathode	90	H_2/O_2	2
Nanoimprint of the protonated Nafion 117 membrane	2.5	0.0005	5	60	H_2/O_2	1
AAO template, Nafion array	1240	70.5	0.0176 at anode	80	H_2/O_2	**This work**

SI-23. References

1. Y. Zhang, J. Lu, H. S. Zhou, T. Itoh and R. Maeda, *J. Microelectromech S.*, 2008, 17, 1020-1028.
2. M. Aizawa, H. Gyoten, A. Salah and X. Liu, *J. Electrochem. Soc.*, 2010, 157, B1844.
3. W. Lee and S. J. Park, *Chem. Rev.*, 2014, 114, 7487-7556.
4. H. Liu, J. Gao, M. Xue, N. Zhu, M. Zhang and T. Cao, *Langmuir*, 2009, 25, 12006-12010.
5. A. C. Ferrari, *Solid State Commun.*, 2007, 143, 47-57.
6. S. K. Babu, R. W. Atkinson, A. B. Papandrew and S. Litster, *ChemElectroChem*, 2015, 2, 1752-1759.
7. Z. Xia, S. Wang, L. Jiang, H. Sun, S. Liu, X. Fu, B. Zhang, D. Sheng Su, J. Wang and G. Sun, *Scientific reports*, 2015, 5, 16100.
8. Z. L. Zhou, R. N. Dominey, J. P. Rolland, B. W. Maynor, A. A. Pandya and J. M. DeSimone, *J. Am. Chem. Soc.*, 2006, 128, 12963-12972.
9. A. Omosebi and R. S. Besser, *J. Power Sources*, 2013, 242, 672-676.